HANDBOOK OF FLUID DYNAMICS AND FLUID MACHINERY

VOLUME III: APPLICATIONS OF FLUID DYNAMICS

Edited by

Joseph A. Schetz and Allen E. Fuhs

A WILEY-INTERSCIENCE PUBLICATION

JOHN WILEY & SONS, INC.

New York • Chichester • Brisbane • Toronto • Singapore

Library of Congress Cataloging in Publication Data:

Handbook of fluid dynamics and fluid machinery/editors, Joseph A. Schetz and Allen E. Fuhs.

p. cm.

Includes index.

ISBN: 0-471-14090-2 (Volume III)

ISBN: 0-471-87352-7 (set)

1. Fluid mechanics. 2. Hydraulic machinery. I. Schetz, Joseph A. II. Fuhs, Allen E.

TA357.H286 1996

620.1'06—dc20 95-5671

Printed in the United States of America

10 9 8 7 6 5 4 3 2 1

independent of the tunnel length, L, and the train speed, V_T, especially for the usual R values in the range of 0.1 to 0.2. This has been verified by full scale experiments [Peters (1990)]. T_f decreases with increasing train length, which is in accordance with full-scale results. In comparing full-scale values of T_f from coasting tests with a value calculated with Eq. (23.188), it should be considered that coasting may have an influence on the flow field due to the deceleration of the train. Therefore, German Rail made tests in a tunnel with a grade in the downhill direction so that the train speed V_T remained nearly constant.

The basic configuration of the Channel Tunnel consists of two single-track running tunnels connected at 250 m intervals with cross-connecting tubes called pressure relief ducts. The concept of these ducts results in considerable traction energy savings, lower pressure levels, and reduced cooling load. But, exhaust flows through the ducts, which can be substantial (50 m/s), impinge on the sides of passing trains. The induced forces can be a considerable risk for less, robust containers and freight wagons and for cars on the open upper deck of car carriers. These effects can be reduced by fitting deflectors on the connecting tubes [Gawthorpe (1992)].

23.9 LIGHTER-THAN-AIR VEHICLES

Sam P. Jones and James D. DeLaurier

23.9.1 Aerostatics for Aerostats and Airships

Introduction. The long and romantic history of airships and their contribution to the development of air transportation is well known. Less familiar is the development in recent years of the tethered aerostat as an important vehicle in communications, intelligence gathering, and surveillance. The development of the power tether which transmits electrical power from the ground has been a factor in the success of the latter. The largest of the tethered aerostats exceeds 500,000 cubic feet in volume and flies routinely at altitudes of 15,000 ft [Krausman (1991)]. The design and operation of these vehicles, both powered airships and tethered aerostats, depend upon environmental and other factors which fall under the general heading of *Aerostatics*. The few references on this subject include Brown and Speed (1962), Durand (1934), Myers (1969), Wright (1976), and Jones (1986). Much of this discussion is taken from the last of these. It is the objective of this section to present an overview of this field sufficient for the engineer to understand the important factors affecting these vehicles and to make elementary calculations of their static performance.

Strictly speaking, aerostat is a generic term applying to both airships and tethered lighter-than-air craft. In the context of this discussion, the airship is considered to be a powered, controlled, ligher-than-air vehicle, while the tethered aerostat, although of aerodynamic shape, is unpowered and tethered to the ground. The same principles of aerostatics apply to both, however the latter is more sensitive to environmental factors, since it flies much higher than the airship and, having no active controls, must be both statically and dynamically stable. The airship seldom flies above 5,000 ft and can overcome inherent instability with active controls.

The Atmosphere. All lighter-than-air vehicles must allow for the expansion of the lifting gas (usually helium) which is determined by the temperature and pressure or density of the external air. An accurate model of the atmosphere is, therefore, es-

sential to prediction of their performance. The effect of ambient conditions is so strong that it is usually not sufficient to use Standard Atmosphere Tables [NOAA (1976)]. A fairly accurate model of the atmosphere is derived from the hydrostatic equation and the usually linear temperature gradient, with the surface conditions as a boundary.

$$dp = -\gamma\, dH \tag{23.190}$$

$$T = T_s - aH \tag{23.191}$$

Here, H is the altitude, p is the pressure, T is the absolute temperature, γ is the specific weight of air, a is the atmospheric lapse rate, and the subscript s denotes surface conditions.

Integration yields

$$p = p_s \left[\frac{T}{T_s}\right]^n \tag{23.192}$$

$$\gamma = \gamma_s \left[\frac{T}{T_s}\right]^{n-1} \tag{23.193}$$

where

$$n = \frac{\gamma_0 T_0}{p_0 a} \tag{23.194}$$

Standard conditions at sea level are the following.

$$p_0 = 1013.25\ mbar = 29.921 \text{ in. Mercury} = 2116.22 \text{ lb/sq ft}$$

$$T_0 = 15 \text{ C} = 59 \text{ F} = 288.15 \text{ K} = 518.67 \text{ R}$$

$$a_0 = .0065 \text{ C/m} = 0.0035662 \text{ F/ft}$$

Under these conditions,

$$\gamma_0 = 1.2250 \text{ kg/cu m} = .076474 \text{ lb/cu ft}$$

$$\lambda_0 = 1.0559 \text{ kg/cu m} = 0.06592 \text{ lb/cu ft}$$

$$n_0 = 5.2558$$

where λ_0 is the specific lift of pure helium.

If the surface is at sea level, then H is the *geopotential altitude* and Eqs. (23.191), (23.192), and (23.193), with n_0 will generate the Standard Atmosphere tables.

The presumption is dry air. The effect of humidity is to reduce the air density which is accounted for by use of *virtual temperature*, T_v. This is the temperature at which the dry air would have the same density as the moist air at the same pressure. It can be calculated using the following formula

$$T_v = \frac{T}{1 - 0.3779 p_w/p} \tag{23.195}$$

where p_w is the partial pressure of water vapor.

Ballonets. An essential feature of both types of lighter-than-air craft is the presence of one or more *ballonets*, which are internal air chambers into which air is pumped or from which it is expelled to maintain pressurization as the temperature and pressure change. Tethered aerostats usually have one large ballonet, while airships more often have two or more. In the latter, they are frequently located fore and aft and used for trim purposes by shifting air from one to the other.

The size of the ballonet or ballonets determines the maximum altitude of the aerostat, since the helium expansion from the ground to altitude must be accommodated. The total ballonet size can be calculated using

$$\frac{V_b}{V_h} = 1 - \frac{(T_s)_{\min}(p_H)_{\min}}{(T_H)_{\max}(p_s)_{\max}} \tag{23.196}$$

Here, V_b is the ballonet volume, V_h is the volume available for helium when the ballonets are empty, $(T_s)_{\min}$ is the minimum temperature on the ground, $(T_H)_{\max}$ is the maximum temperature at maximum altitude and $(p_H)_{\min}$ and $(p_s)_{\max}$ are the helium pressures.

The large TCOM* 71 meter aerostat designed to carry a 3500 lb payload to 15,000 ft has a ballonet volume of 56% of the hull volume, while the Westinghouse** Sentinel 1000 airship's ballonets are 24% of the total volume.

The large ballonets of tethered aerostats present a special problem in the calculation of static trim and center of gravity. The ballonet air, being much heavier than the helium, tends to form a level surface, as shown in Fig. 23.96. This causes a variable center of gravity depending upon the volume of air and pitch angle. The problem is very minor in the much smaller ballonets of airships and is usually ig-

*TCOM, L.P., Columbia, MD.
**Westinghouse Airships, Inc., Baltimore, MD.

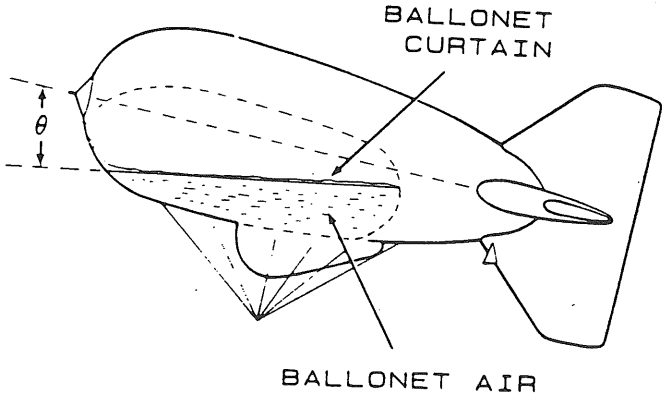

FIGURE 23.96 Leveling of air in the ballonet of a tethered aerostat.

nored. For large tethered aerostats, however, a family of curves must be prepared for each design showing the centroid of the ballonet air as a function of fullness and pitch angle. These are usually expressed as a family of polynomials used in both static and dynamic analyses.

Buoyancy Model. For dynamic analysis, the *Archimedean buoyancy* of the entire body and the total mass, including the enclosed gases, must be considered. This presents the difficulties due to air in the ballonets of large aerostats discussed in the preceding paragraph. A simplified model, commonly used for steady-state analysis, envisions the lifting gas as free to expand by expelling neutrally-buoyant air from the ballonet. In this model, the gross buoyant lift is that of an independent parcel of helium. Neglecting the small pressure differential (*superpressure*) and with no temperature differential relative to the ambient (*superheat*), the lift of such a parcel is independent of temperature and pressure and therefore of altitude. This is due to the fact that the specific lift of the gas decreases in exactly the same proportion as the volume increases. This model has the added advantage that the gross weight is that of the structure alone, which has a fixed weight, and center of gravity. The variable is the center of buoyancy, the centroid of the helium volume, calculated from the ballonet polynomials.

This simple model requires corrections for deviations from the simplifying assumptions that the internal gases are at the same temperature and pressure as the surrounding air and that both are dry. The gross lift of the helium thus corrected is referred to as the *Standard Gross Lift*.

Correction for Superpressure: The superpressure is the differential of the pressure inside the hull to the ambient and is responsible for maintaining the rigidity of the hull. Common practice for both airships and tethered aerostats is to maintain about 2 in. of water gauge above dynamic pressure. This compression of the enclosed gases results in a loss of lift, ΔL_p, given by

$$\Delta L_p = -\gamma V_t \frac{\Delta p T}{p T_g} \tag{23.197}$$

which reduces to

$$\Delta L_p = -\frac{\gamma_0 T_0 V_t}{p_0} \frac{\Delta p}{T_g} \tag{23.198}$$

where V_t and T_g are the total volume and temperature of the enclosed gases.

Since the absolute temperature does not vary greatly, the lift loss is almost independent of altitude. For a 500,000 cu ft vehicle with a superpressure of 2 in. water gauge, the lift loss would be about 195 lb.

Correction for Superheat: The term *superheat* in common usage refers to the temperature differential of the internal gases to the ambient air. It results from the radiation environment and is usually positive in the daytime due to solar radiation and negative at night when the aerostat radiates to a clear sky. The effect is maximum during clear, calm conditions when the heat exchange with the environment is by

natural convection. Relative wind diminishes superheat due to the forced convection heat transfer. For that reason, the effect is much less important for airships except when moored, since they create their own relative wind.

Superheat has two effects. It increases the volume of helium, expelling air from the ballonets, and increases the lift by decreasing the density of the enclosed gases. Assuming the enclosed gases are at a uniform temperature, the net effect on buoyant lift is analogous to that for superpressure.

$$\Delta L_l = \gamma V_l \frac{\Delta T}{T_g} \tag{23.199}$$

For a 500,000 cu ft vehicle at 5000 ft altitude, the effect amounts to a gain of about 65 lb per degree F of superheat.

The magnitude of superheat depends upon many factors including the hull material, time of day, cloud cover, season, and relative wind. Figure 23.97 presents data taken on a TCOM 250 tethered aerostat at Grand Bahama Island during an unusual period of clear, calm conditions for two days in January 1974. The wind velocity was less than 5 knots, and the aerostat's altitude was maintained between 8500 and 10,800 ft. The shielded temperature probe was hanging about 15 ft from the top of the hull at the major diameter [Jones (1986)]. Like all subsequent TCOM aerostats, the laminated hull material included an outer layer of white Tedlar® film. During the day, subjected to solar radiation, the helium temperature reached about 25°F higher than the ambient air, while at night, due to radiation to space, the differential was negative by more than 10°F. These results are fairly typical of observations with other aerostats under similar conditions, irrespective of location and season.

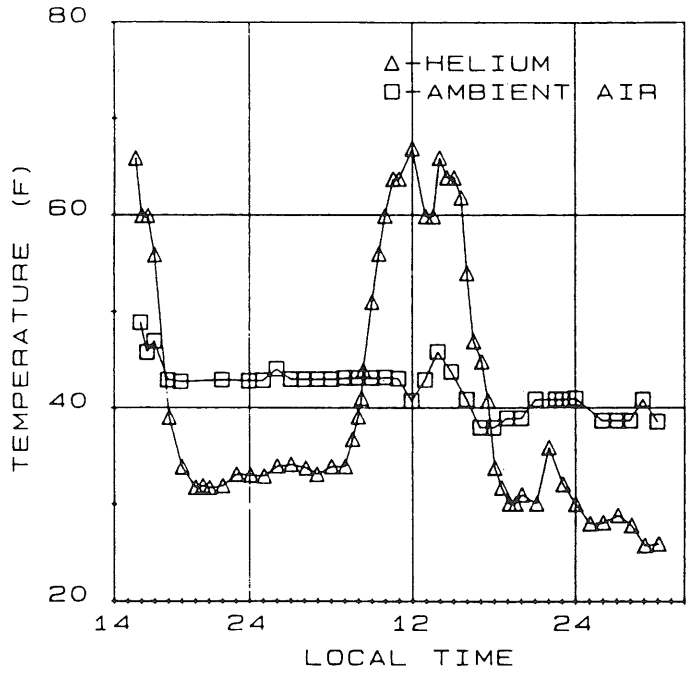

FIGURE 23.97 Helium and air temperature on a TCOM 250 aerostat during calm conditions, Grand Bahama Island, Jan. 18–20, 1974.

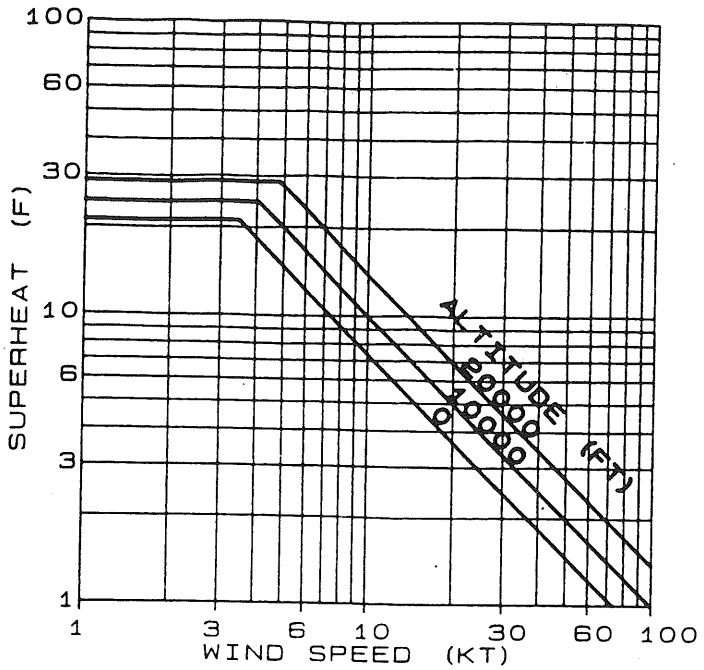

FIGURE 23.98 Semiempirical curves for estimating day superheat.

Based upon empirical data and heat transfer theory, the curves of Figs. 23.98 and 23.99 have been derived to estimate the superheat for day and night conditions, respectively. At low winds, free convection is assumed, and at higher winds cooling is primarily by forced convection.

The Effect of Humidity: Water vapor is lighter than air, so moist air provides less buoyant force on immersed bodies than dry air. This may be offset, however, by

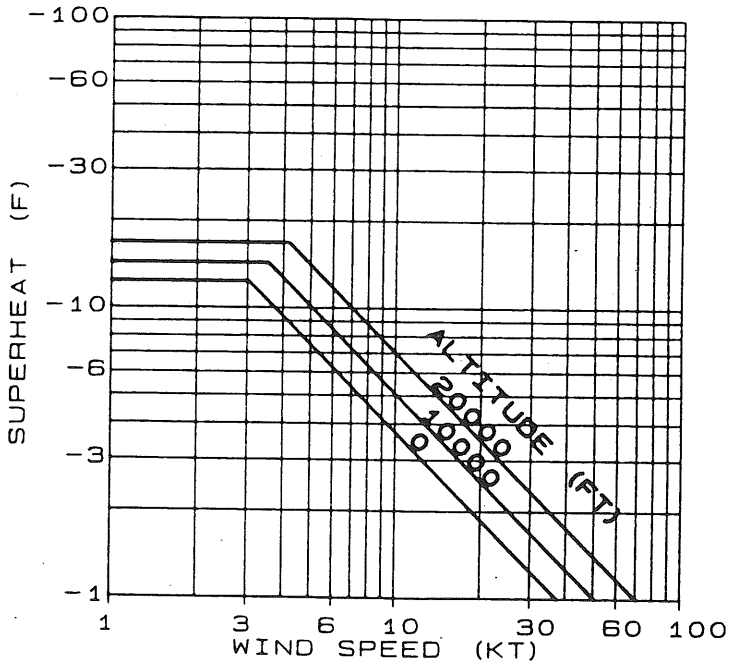

FIGURE 23.99 Semiempirical curves for estimating negative superheat at night.

water vapor inside the aerostat. A little known fact is that, although relatively impermeable to helium, most modern tethered aerostat and airship materials transmit water vapor rather well. Thus, tests on TCOM laminated hull material using ASTM E-398 gave a water vapor transmissivity of 1.3 grams per 100 sq in. per 24 hr at 100 F [Ashford *et al.* (1983)]. This is over 10 times the helium permeability measured at the same temperature when compared on the same basis.

While moisture in the ambient air decreases lift, water vapor inside the hull, being lighter than air, increases lift. The water vapor content inside the hull will approach that of the outside air, in which case, there will be no net effect on lift. For that reason and the difficulty of measuring the humidity in helium, this effect is usually ignored. However, ambient humidity fluctuates widely and water vapor change inside the hull lags by many hours so that the concentrations are seldom the same. Humidity should be taken into account when making precise measurements such as lift loss rate.

Figure 23.100 shows the effect of water vapor in both the air and the helium on the gross lift factor or ratio to the lift of dry helium [Jones (1986)]. The curves are given in terms of the dew point, which is a measure of water vapor content with a single number.

In addition to the effect on buoyant lift, water vapor in the helium affects the maximum altitude of the aerostat. Since it occupies volume, the altitude at which the ballonets are empty will be lowered.

Aerostatic Flight Envelopes. Both airships and tethered aerostats are limited in their maximum altitude and the temperature and pressure when moored by the helium fill (gross lift) and size of the hull and ballonets. In airship parlance, the maximum altitude is known as the *pressure height*, H_p. It is the altitude at which the helium has expanded to expel all the air in the ballonets and any further increase in altitude would cause a dangerous increase in hull pressure or venting of the helium. Thus, it is sometimes called the *vent ceiling*.

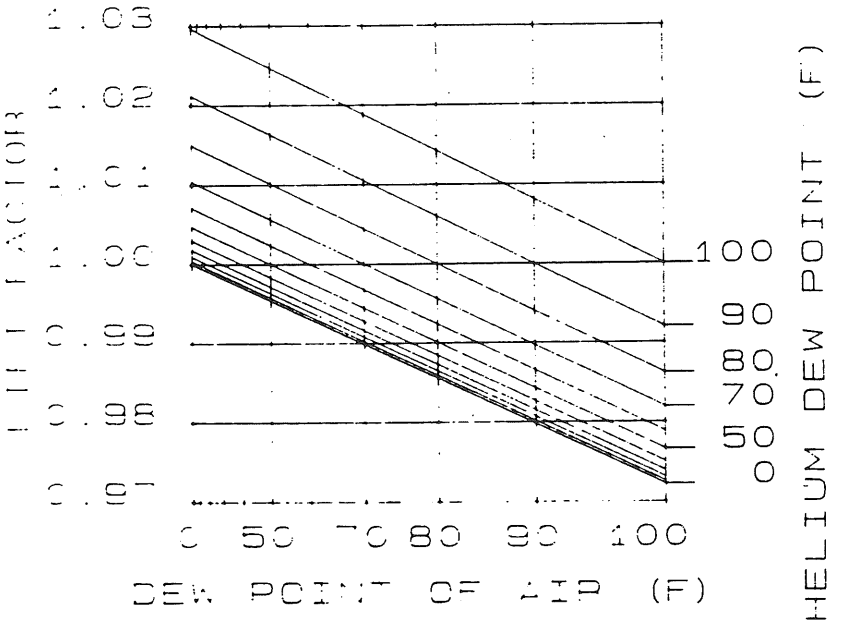

FIGURE 23.100 Nomograph showing the effect of water vapor on helium gross lift.

Making use of Eq. (23.193) and the gas laws, and neglecting the small superheat and superpressure, the pressure height of an airship is given by

$$H_p = \frac{T_s}{a}\left[1 - \left(\frac{Lp_0T_s}{V_h\lambda_0 f_p p_s T_0}\right)^{1/(n-1)}\right] \tag{23.200}$$

where L is the standard gross lift of helium, and f_p is the helium purity expressed as volume fraction.

At low altitudes, as when moored, and low temperatures, the helium may contract to such a small volume that the ballonets are completely filled with air. This is the lower limit of helium volume.

$$V_f = V_h - V_b \tag{23.201}$$

This altitude can be found by substituting V_f for V_h in Eq. (23.200).

While the same equations apply to tethered aerostats, their ceiling altitude must take into account the weight of the tether and the much higher superheat and relative superpressure at the higher altitudes. In addition, tethered aerostats require significant free lift or excess buoyancy over that required to lift the system including the tether. It is essential to know how high the aerostat can safely fly under calm conditions and what helium fill must be provided. The operating altitude is determined by two factors, illustrated in Fig. 23.101, which is a plot of altitude as a function of helium fill in terms of gross lift. The curves of positive slope represent the lift limit for the gross weight, including tether and free lift. The greater the altitude, the greater the tether weight and thus the more lift required. The slope is the inverse of the unit weight of the tether. At night, negative superheat reduces lift, as shown by the displaced curve.

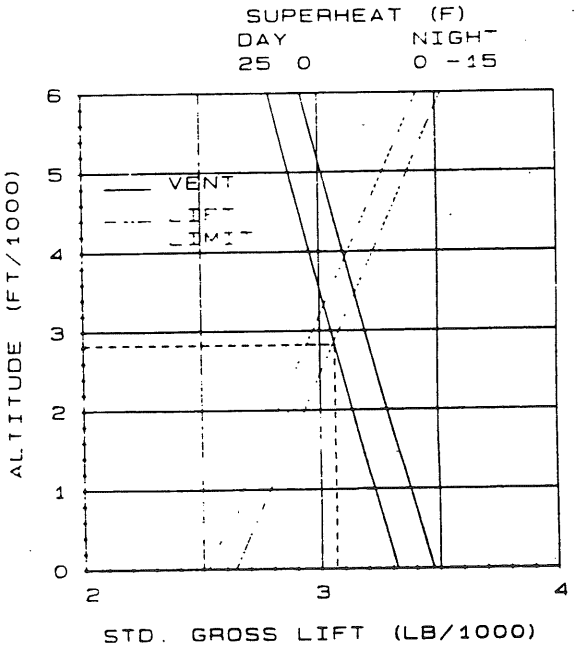

FIGURE 23.101 Vent altitude and lift limit curves for determining optimum altitude and lift (dashed lines).

The second factor determining operating altitude is the pressure height or vent ceiling, represented by the curves of negative slope. This curve is very sensitive to superheat, which reduces the pressure height.

The intersection of the lift limit and vent ceiling curves gives the altitude that can be maintained both day and night with a minimum specified free lift and allowances for superheat. This is known as the *optimum altitude*, and the corresponding gross lift is the *optimum helium fill*. Of course, wind reduces superheat and provides aerodynamic lift, so it will be possible to fly higher than the optimum altitude under some conditions, but that will be at the expense of free lift based on helium buoyancy. For flights of many days, it may be necessary to compromise altitude by overfilling to account for helium leakage.

Figure 23.101 is specific for a given set of ambient conditions. In particular, the ambient temperature and pressure will affect the vent ceiling. Figure 23.102 shows how the optimum altitude varies with sea level temperature for the TCOM 31-meter tethered aerostat, with payload weight as a parameter. Standard sea level barometric pressure and lapse rate are assumed. The free lift is 20% of the gross lift, and the daytime superheat is taken to be 25°F. The negative superheat at night is not taken into account. It is a matter of strategy to ignore negative superheat, which only exists under calm conditions.

23.9.2 Aerodynamics for Aerostats and Airships

For a traditional configuration consisting of an axisymmetric body with aft fins, as shown in Fig. 23.103, a lighter-than-air vehicle's steady-state normal force, axial force, and pitching moment may be calculated from a modified cross-flow analysis. In this, it is assumed that the vehicle is divided into two distinct aerodynamic regions—the hull, which extends from the nose to the hull-fin intersection point, l_h,

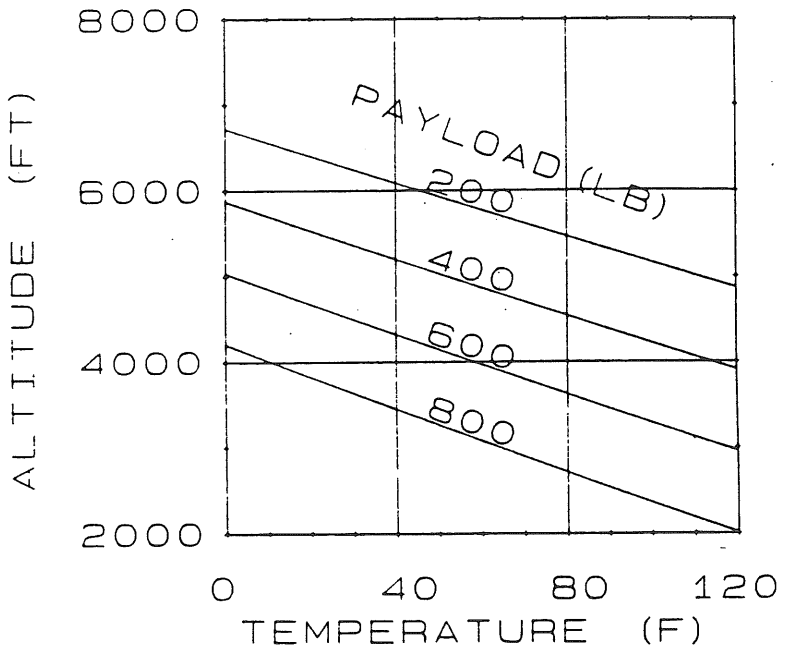

FIGURE 23.102 Optimum altitude as a function of sea-level temperature for the TCOM 31 meter aerostat with various payloads. Free lift is 20% of the gross lift.

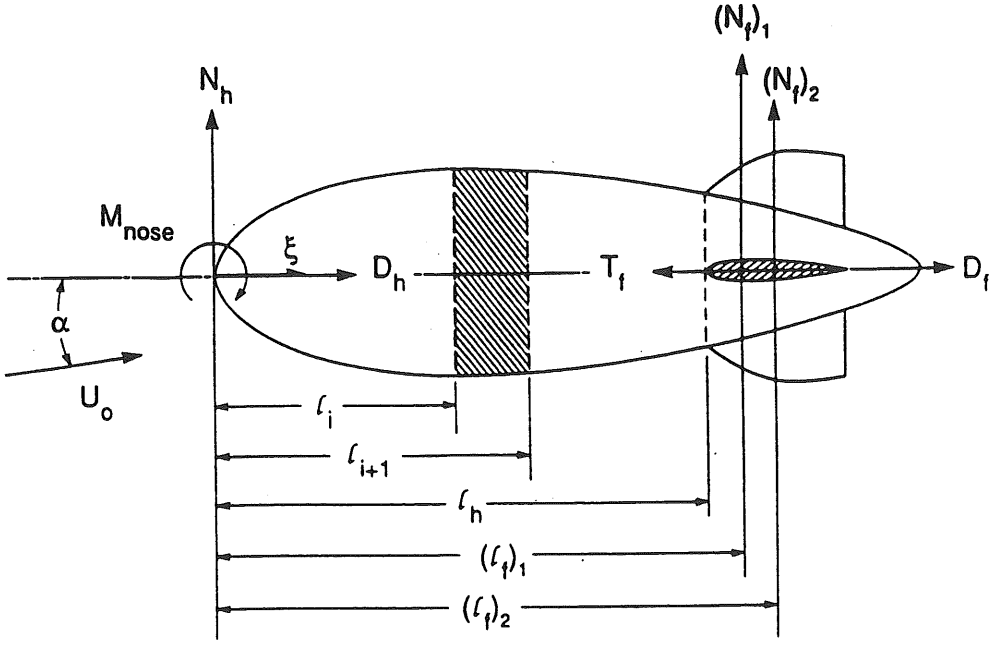

FIGURE 23.103 Schematic of analytical model.

and the fins, which continue from that point to their trailing edge. For nonseparated flow, the hull forces and moment are obtained from Allen and Perkins (1951), and the fins' normal force is obtained from Wardlaw (1979), with efficiency factors, η_k and η_f, introduced to account for mutual interference between hull and fins. From Jones and DeLaurier (1983), the resulting equations are for the normal force

$$\begin{aligned} N &= Cnq_0S \\ Cn &= [(k_3 - k_1)\eta_k\hat{I}_1 + 0.5(Cn^*_\alpha)_f\eta_f\hat{S}_f] \sin(2\alpha) \\ &\quad + [(Cd_c)_h\hat{J}_1 + (Cd_c)_f\hat{S}_f] \sin\alpha \sin|\alpha| \end{aligned} \tag{23.202}$$

and for the axial force

$$\begin{aligned} D &= Cdq_0S \\ Cd &= [(Cd_h)_0\hat{S}_h + (Cd_f)_0\hat{S}_f] \cos^2\alpha \\ &\quad - (k_3 - k_1)\eta_k\hat{I}_1 \sin(2\alpha) \sin(\alpha/2) - (Ct)_f\hat{S}_f \end{aligned} \tag{23.203}$$

The pitching moment (about the nose) is

$$\begin{aligned} M_{nose} &= Cm_{nose}q_0S\bar{c} \\ Cm_{nose} &= -[(k_3 - k_1)\eta_k\hat{I}_3 + 0.5(\hat{l}_f)_1(Cn^*_\alpha)_f\eta_f\hat{S}_f] \sin(2\alpha) \\ &\quad - [(Cd_c)_h\hat{J}_2 + (Cd_c)_f(\hat{l}_f)_2\hat{S}_f] \sin\alpha \sin|\alpha| \end{aligned} \tag{23.204}$$

The terms in these equations are defined as follows: q_0 = free-stream dynamic pressure = $\rho(U_0)^2/2$, S = (total hull volume)$^{2/3}$, the reference area; $\bar{c}$ = total hull length,

the reference length; α = the angle of attack of the vehicle's center-line to the free stream flow direction; k_1, k_3 = axial and lateral apparent-mass coefficients, respectively, given by

$$k_1 = \gamma/(2 - \gamma); \qquad k_3 = \delta/(2 - \delta)$$

$$\gamma = 2\left(\frac{1 - e^2}{e^3}\right)\left[\frac{1}{2}\ln\left(\frac{1 + e}{1 - e}\right) - e\right]$$

$$\delta = \frac{1}{e^2} - \frac{1 - e^2}{2e^3}\ln\left(\frac{1 + e}{1 - e}\right)$$

$$e = \left(\frac{f^2 - 1}{f^2}\right)^{1/2} \tag{23.205}$$

where f, the hull's fineness ratio, is f = total hull length/hull maximum diameter The nondimensional hull integrals, $\hat{I}_1$, $\hat{I}_3$, $\hat{J}_1$, and $\hat{J}_2$, are given by

$$\hat{I}_1 = \frac{1}{S}\int_0^{l_h} \frac{dA}{d\xi}\, d\xi = \frac{A_h}{S}; \qquad \hat{I}_3 = \frac{1}{S\bar{c}}\int_0^{l_h} \xi \frac{dA}{d\xi}\, d\xi$$

$$\hat{J}_1 = \frac{1}{S}\int_0^{l_h} 2r\, d\xi; \qquad \hat{J}_2 = \frac{1}{S\bar{c}}\int_0^{l_h} 2r\xi\, d\xi \tag{23.206}$$

where A = hull cross-sectional area, ξ = axial distance along the hull, measured from the nose, and r = hull radius.

Also,

$\hat{S}_f = S_f/S$, nondimensional fins' reference area (see Fig. 23.104 for S_f).
$\hat{S}_h = S_h/S$, the nondimensional hull reference area [usually $S_h = S$, depending how $(Cd_h)_0$ is defined].
$(Cd_h)_0$ = hull zero-angle axial drag coefficient, referenced to S_h. [This includes skin friction, base drag, and excrescence drag. A good reference for estimating these values is Hoerner (1965).]
$((Cd_f)_0)$ = fin's zero-angle axial drag coefficient, referenced to S_f. (This involves the profile drag of the exposed surfaces, as well as the interference drag where the roots of the fins intersect the hull.)

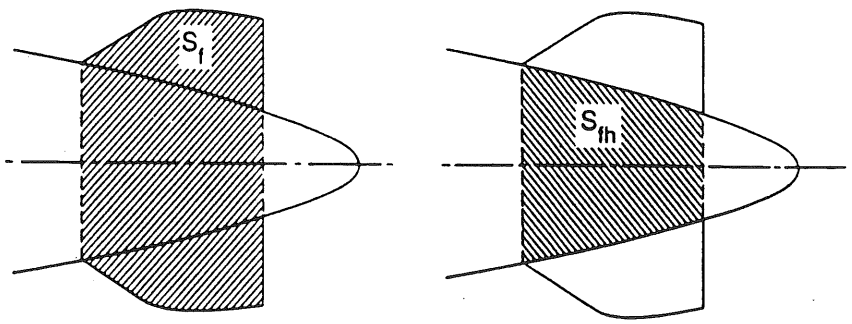

FIGURE 23.104 Fin planform definition.

$(Cd_c)_h$ = hull cross-flow drag coefficient, referenced to $\hat{J}_1 S$. [From Wardlaw (1979), this value is typically ≈ 0.3.]

$(Cd_c)_f$ = fin's cross-flow drag coefficient, references to S_f.

Plots for $(Cd_c)_f$ are presented in Wardlaw (1979), which are summarized in the following curve-fitted equations

$$(Cd_c)_f = A_0 + A_1 \times AR + A_2 \times AR^2 + A_3 \times AR^3 \qquad (23.207)$$

for $0 < AR \leq 3$ and where

$$A_0 = 2.008 + 3.99\lambda \qquad A_1 = -0.832 - 3.289\lambda + 0.7885\lambda^2$$
$$A_2 = 0.185 + 2.028\lambda - 1.15\lambda^2 \qquad A_3 = -0.0178 - 0.44\lambda + 3.2\lambda^2 \qquad (23.208)$$

In these, AR = the fins' aspect ratio, defined by $AR = b^2/S_f$ (it is important to note that, for fins with a dihedral angle, Γ, that b is twice the semi-span length from the hull's center-line to the fin's tip. In other words; it is *not* the projected length on the horizontal plane) and λ = the fins' taper ratio. (Since the effective planform, shown by S_f in Fig. 23.104, does not generally have a simple straight taper, it has been found adequate to chose an equivalent straight-tapered planform as shown in Fig. 23.105.) For the purposes of initial estimations, a representative $(Cd_c)_f \approx 2.0$ for the AR and λ values typical for airship and aerostat fins.

$(Cn^*_\alpha)_f$ is the derivative of the isolated fins' normal-force coefficient with respect to α, at $\alpha = 0$ and referenced to S_f. A useful equation for estimating this is obtained from Lowry and Polhamus (1957), with a correction factor to account for the horizontal fins' dihedral angle

$$(Cn^*_\alpha)_f = \frac{2\pi AR \cos^2 \Gamma}{2 + \left[\frac{(AR)^2}{\kappa^2}(1 + \tan^2 \Lambda_{c/2}) + 4\right]^{1/2}} \qquad (23.209)$$

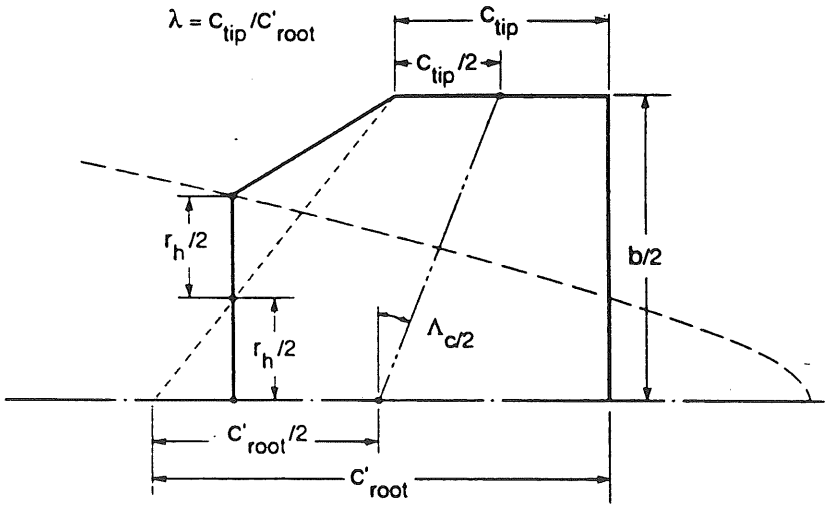

FIGURE 23.105 Equivalent straight-tapered planform.

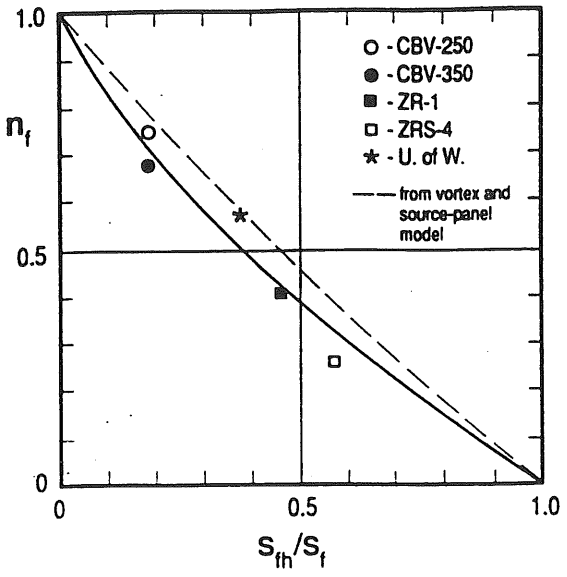

FIGURE 23.106 Fin-efficiency factor.

where

$\Lambda_{c/2}$ = sweep of the half-chord line of the equivalent straight-tapered planform, shown in Fig. 23.105.

κ = ratio of the airfoil section's lift-curve slope to 2π (a reasonable estimate is $\kappa \approx 0.95$).

Γ = fins' dihedral angle.

η_f = fin-efficiency factor accounting for the effect of the hull on the fins, given as a function of S_{fh}/S_f in Fig. 23.106 (S_{fh} = portion of the fins' area covered by the hull, as shown in Fig. 23.104). η_k = hull-efficiency factor accounting for the effect of the fins on the hull, given as a function of $S_f \cos^2(\Gamma)/(J_1)_{\text{total}}$ in Fig. 23.107 [$(J_1)_{\text{total}}$ = the value of $\hat{J}_1 S$ when the integral for $\hat{J}_1$ extends to the end of the hull. Note that this is the hull's complete horizontal projected area (*shadow area*)].

Curves for η_k and η_f, shown in Figs. 23.106 and 23.107, were obtained from a semi-empirical method based on wind tunnel data for several airship and aerostat

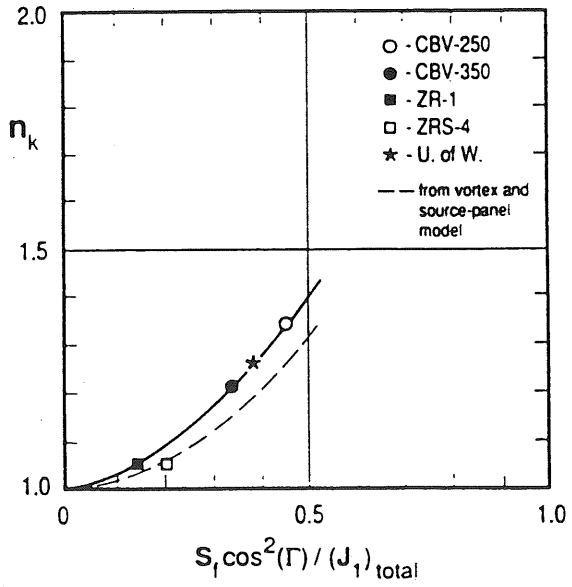

FIGURE 23.107 Hull-efficiency factor.

models as described in Jones and DeLaurier (1983). Subsequently, these curves were rederived by Wong, Zhiyung, and DeLaurier (1985) by using a vortex and source-panel computational model. The results are co-plotted on Figs. 23.106 and 23.107, where it is seen that they are a reasonably close match. Good results have been obtained from using the semi-empirical curves.

$(C_t)_f$ = the fins' leading-edge suction coefficient, given by

$$(Ct)_f = (Cn_\alpha^*)_f \eta_f \eta_l \frac{\sin(2\alpha)}{2} \tan\alpha - \frac{[(Cn_\alpha^*)_f \eta_f \sin(2\alpha)]^2 \eta_l}{4\pi AR} \qquad (23.210)$$

where

η_l = the leading-edge suction efficiency (For fins incorporating airfoils with rounded leading edges, $\eta_l \approx 1.0$. However, fins with sharp leading edges may give an $\eta_l \approx 0$)

and finally

$(\hat{l}_f)_1 = (l_f)_1/\bar{c}$, nondimensionalized distance from the hull's nose to the fins' aerodynamic center (based on the S_f planform)

$(\hat{l}_f)_2 = (l_f)_2/\bar{c}$, nondimensionalized distance from the hull's nose to the fins' center of cross-flow force (the area center of the exposed fins, $S_f - S_{fh}$)

This method was applied by Badesha and Jones (1993) to the CBV 71M aerostat shown in Fig. 23.108. This incorporates three identical fins arranged in an inverted-Y configuration, where $\Gamma = -45°$. The values of the parameters for this aerostat are: $\hat{S}_h = 1.0$, $\hat{S}_f = 0.8369$, $\hat{I}_1 = 0.2090$, $\hat{J}_1 = 1.5542$, $\hat{I}_3 = -0.1691$, $\hat{J}_2 = 0.5498$, $(Cn_\alpha^*)_f = 2.7101$, $(\hat{l}_f)_1 = 0.8108$, $(\hat{l}_f)_2 = 0.8798$, $(k_3 - k_1) = 0.7169$, $\eta_f = 0.6684$, $\eta_k = 1.0034$, $(Cd_c)_f = 1.1145$, $(Cd_c)_h = 0.1200$, $S_{fh}/S_f = 0.2851$, $S_f \cos^2\Gamma/(J_1)_{\text{total}} = 0.2329$ and the resulting normal force and pitching coefficients are co-plotted with results from wind tunnel tests in Figs. 23.109 and 23.110.

The aerostat in Fig. 23.108 has a very small portion of hull extending aft of the fins' trailing edge. However, blimps and airships are characterized by larger aft hull portions (commonly called the *boat tail*), as drawn in Fig. 23.103. It has been found that, for this analysis, only the boat tail's skin friction and base drag contribution

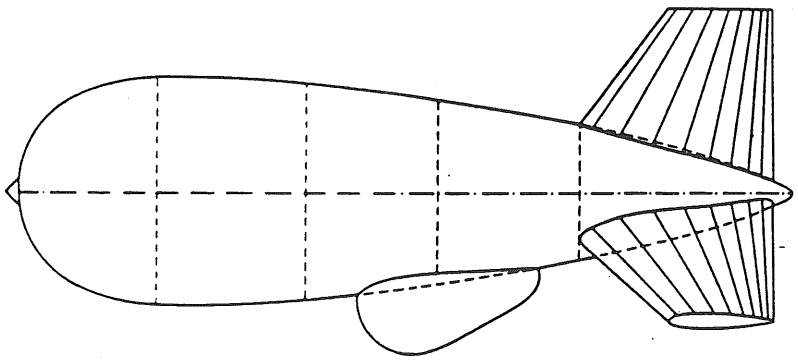

FIGURE 23.108 Aerostat CBV 71M.

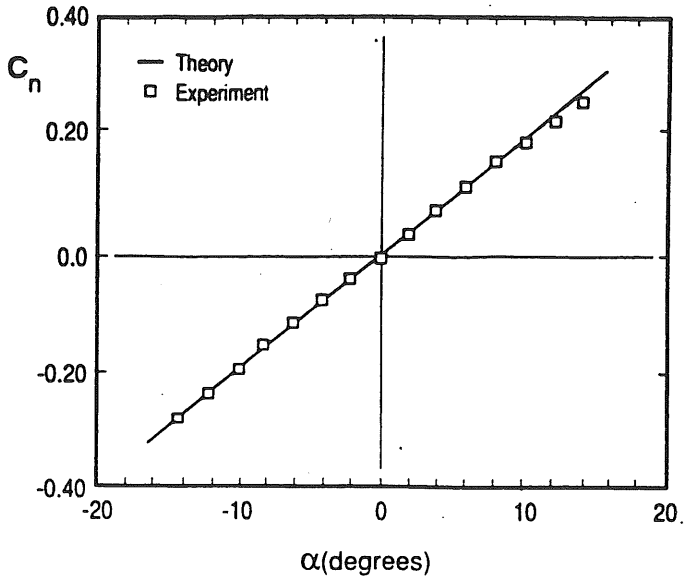

FIGURE 23.109 Results for Cn vs. α.

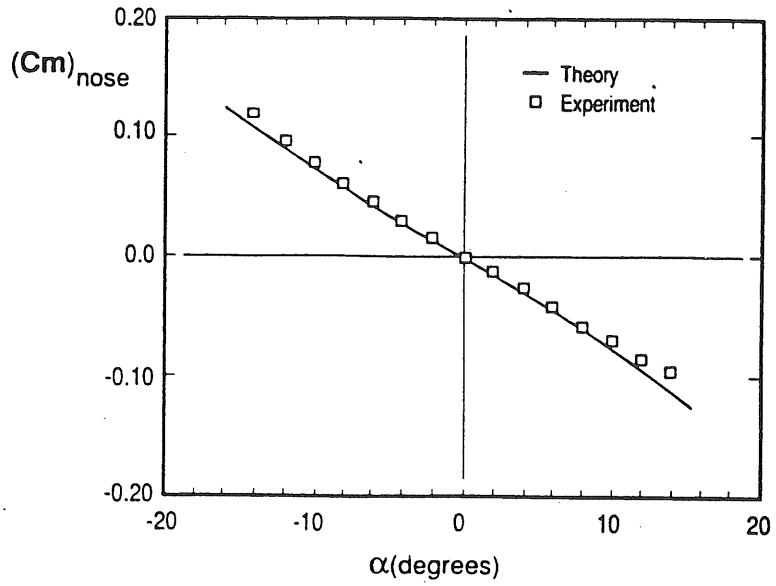

FIGURE 23.110 Results for $(Cm)_{nose}$ vs. α.

[through the $(Cd_h)_0$ term] need be accounted for. The flow straightening effect of the fins essentially eliminates any cross flow in the boat-tail region.

23.10 LAMINAR FLOW CONTROL ON AIRCRAFT

Fayette S. Collier, Jr.

23.10.1 Introduction

Drag reduction in the form of laminar flow control applied to future, advanced commercial, and military transports across the speed regime offers potential breakthrough opportunities in terms of reductions in takeoff gross weight (TOGW), operating empty weight (OEW), block fuel for a given mission, and significant